JOURNAL OF OPTOELECTRONICS AND ADVANCED MATERIALS Vol. 9, No. 6, June 2007, p. 1757 - 1761

Section 8. Advanced Materials. General aspect
Invited Paper

Nanocrystalline iron based-alloys

E. BURZO*, C. DJEGA-MARIADASSOU[a]
Faculty of Physics, Babes-Bolyai University 400084 Cluj-Napoca, Romania
[a]LCMTR UPR 209 CNRS 2/8 Bat. F RueHenry Dunant 94320 Thiais, France

The magnetic properties of nanocrystalline $Sm_2Fe_{17-x}Si_xC_2$ alloys were studied in the temperature range 4.2-800 K and fields up to 10 T. The saturation magnetizations are little higher than in noncarbonated systems having the same composition. The $\Gamma = d\ln T_c/d\ln v$ values show linear dependences on the Curie temperature, T_c, suggesting that iron moments are mainly localized. The $\gamma=d\ln J_{eff}/d\ln v=16.4$, a value close to that determined in highly carbonated $R_2Fe_{17}C_x$ polycrystalline compounds where R is a rare-earth or yttrium. Band structure calculations show linear dependences of Fe moments, as well as of R5d band polarizations on De Gennes factor. The magnetic properties of $Nd_6Fe_{88-x}M_xB_6$ nanocomposites with M=V or Fe were also studied. Remanent inductions B_r = (0.62-0.67) were obtained.

(Received November 14, 2006; accepted April 26, 2007)

Keywords: Nanocrystalline alloys, Crystal structures, Magnetic properties

1. Introduction

The nanocrystalline alloys have interesting properties with possible technical applications. Particularly, iron based systems, as function of composition, show either hard or soft magnetic properties. Previously, we studied the physical properties of nanocrystalline $Sm_2Fe_{17-x}Si_x$ [1], $SmFe_{9-y}Si_yC_z$ with z = 0,1 [2,3] and nanocomposites based on Nd-Fe-B [4] as possible new hard magnetic materials. Particularly, $SmFe_{9-y}Si_yC_z$ alloys have high coercive force and saturation magnetizations.

The Curie temperature of Sm_2Fe_{17} is rather low, T_c=389 K, and the anisotropy is planar [4]. Although the mean iron moment is close to that of pure iron, the above compound cannot be used as permanent magnet. The low Curie temperature of Sm_2Fe_{17} is connected with the site occupancy of iron in $R\bar{3}m$-rhombohedral lattice. For smaller distances between iron atoms than $\cong$ 2.50 Å, the exchange interactions are negative, whereas those between Fe atoms situated at larger distances than the above value are positive. The negative exchange interactions are not satisfied since they are smaller than the positive ones and consequently a considerable magnetic energy is stored. A strong decrease of the Curie temperature results.

In order to analyse the effect of both silicon substitutional effect and of interstitial C atoms on Curie temperatures and anisotropies, the physical properties of $Sm_2Fe_{17-x}Si_xC_2$ were studied. By Si substitution we expect a reduction of the number of Fe-Fe antiferromagnetic pairs. In addition, the lattice dilatation, consequence of the presence of interstitial carbon, will also contribute to the decrease of negative exchange interactions. These can lead to the increase of the Curie temperatures.

We analyse also the magnetic properties of $Nd_6Fe_{88-y}M_yB_6$ nanocomposites with M = Fe and V and y=1. This system is expect to be composed of hard magnetic phase based on $Nd_2Fe_{14}B$ and α-Fe and/or Fe_3B soft magnetic particles. The increase in remanence, due to nanoscale structure, may be further enhanced by the presence of the soft magnetic phases [6].

2. Experimental and Computing Method

The $Sm_2Fe_{17-x}Si_x$ nanocrystalline alloys were prepared by high energy ball milling and subsequent annealing. The Sm-Fe prealloyed powders and silicon powders were milled 5 hrs and then annealed in silica tube in vacuum of $5\cdot10^{-5}$ torr for 30 min at 1150^0C. By using this method, a better control of the stoichiometry is ensured than by conventional methods. The carbonation was achieved by reaction of the alloy powder with appropriate amount of $C_{14}H_{10}$ powder.

The crystal structure were analysed by X-rays. Rietveld refinement was performed by using a FULLPROF computer code with a peak line profile of Thompson-Cox-Hastings [1]. The silicon was shown to occupies the 18h sites. The composition dependences of the lattice parameters are given in Fig.1. The lattice constants in carbonated samples are higher by 2.4 – 2.6 %, comparatively to noncarbonated ones. The lattice parameters decrease slightly when increasing silicon content. The mean grain sizes are situated between 18 and 25 nm.

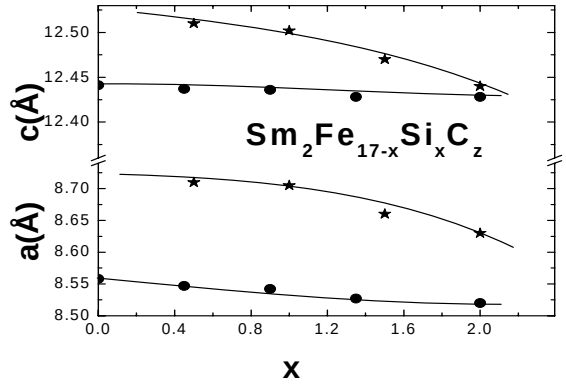

Fig. 1. Composition dependences of the lattice parameters of $Sm_2Fe_{17-x}Si_xC_z$ with z = 0(•) and 2(*).

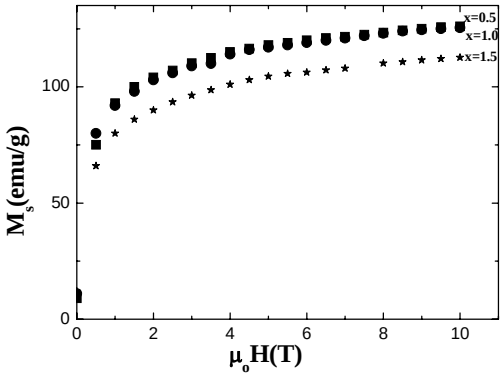

Fig. 2. Magnetization isotherms at 4.2 for $Sm_2Fe_{17-x}Si_xC_2$ alloys.

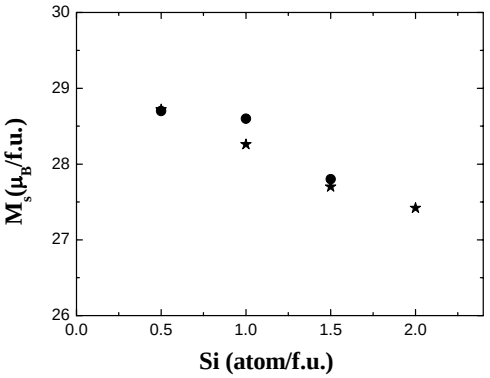

Fig. 3Composition dependences of the saturation magnetizations for $Sm_2Fe_{17-x}Si_xC_z$ alloys with z = 0(*) and 2 (•).

The $Nd_6Fe_{88-y}M_yB_6$ samples with M=V,Fe and y=1 were prepared by splat cooling. The wheel speed was 25 m/s. The presence of some α-Fe and Fe_3B crystalline phases in an amorphous matrix was shown. The samples were thermally treated in vacuum of $1\cdot10^{-4}$ torr at 650^0C up to 5 min. During crystallization, firstly the α-Fe and Fe_3B nanoparticles were shown. Then, the hard magnetic phase crystallized. The distribution of particles was analysed by X-rays and electron microscopy.

Magnetic measurements were performed in the temperature range 4.2-800 K and fields up to 10 T.

Band structure calculations were performed by using the ab initio tight binding linear muffin tin orbital method in the atomic sphere approximation (TB-LMTO-ASA) [7]. In the framework of the local density approximation (LDA), the total electronic potential is the sum of the external, Coulomb and exchange correlation energies [8]. The functional form of the exchange correlation energy, used in the present work, was the free electron gas parametrization of Von Barth and Hedin [9]. Relativistic effects were included. The 4f states were treated as part of core. These electrons are not part of band structure, but the polarization of the 4f densities is calculated self consistently.

3. Experimental results

The magnetization isotherms of $Sm_2Fe_{17-x}Si_xC_2$ alloys, at 4.2 K, are plotted in Fig. 2. The magnetizations are not saturated even in field μ_0H=10 T. This suggest that the anisotropies changed from planar to uniaxial. The saturation magnetizations, M_s, were obtained according to approach to saturation law, $M = M_s(1-a/H)$, by extrapolating the measured values to $H^{-1} \rightarrow 0$. The M_s values thus obtained are plotted in Fig. 3. The saturation magnetizations obtained in case of noncarbonated samples are also given. Generally, the M_s values of carbonated samples are only little higher than those of the noncarbonated ones.

The composition dependences of the Curie temperatures, T_c, for $Sm_2Fe_{17-x}Si_xC_2$ with z = 0 and 2 are given in Fig. 4. The T_c values of the samples having z=0 increase gradually as the silicon content is higher. The above behaviour can be attributed mainly to the reduction of antiferromagnetic interactions, by breaking antiferromagnetic pairs, where $d_{Fe\text{-}Fe}$<2.50 Å, particularly Fe9d-Fe18h and in a smaller extent Fe18h-Fe18h ones. There can be also a filling of the Fe3d band by Si3p electrons implying a shift to strong ferromagnetic behaviour. The Curie temperatures of carbonated samples are substantially higher than of noncarbonated ones. The increase of the lattice parameters leads to Fe-Fe distances greater than ≅ 2.50 Å for all types of Fe atoms. As a result, the negative exchange interactions disappear, the system being characterized only by positive ones. When substituting Fe by Si a decrease of T_c values can be seen. This behaviour can be attributed to magnetic dilution effects which leads to the diminution of ferromagnetic interactions.

The volume effects on the Curie temperatures can be analysed by using the Γ parameter defined by the relation [10,11]:

$$\Gamma = \frac{1}{\kappa T_c} \cdot \frac{dT_c}{dp} = \frac{d \ln T_c}{d \ln v} \qquad (1)$$

We denoted by κ the compressibility and v the cell volume. If the Fe3d electons are considered having mainly a localized behaviour, the Γ value can be described by the relation [10]:

$$\Gamma = \frac{5}{3} + 2\frac{d \ln J_{eff}}{d \ln v} + \frac{5}{8} \cdot \frac{k_B N_o g^2 I}{S(S+1) J_{eff}^2 I_b} \cdot T_c \qquad (2)$$

where N_o is the Avogadro number, g is Landé factor, I is the effective intra-atomic exchange integral which is reduced from its bare value I_b and J_{eff} is the effective exchange parameter.

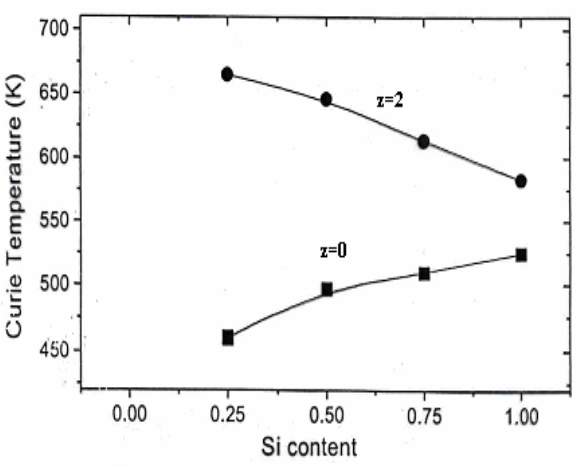

Fig. 4. Composition dependences of the Curie temperatures for $Sm_2Fe_{17-x}Si_xC_z$ with z = 0 and 2.

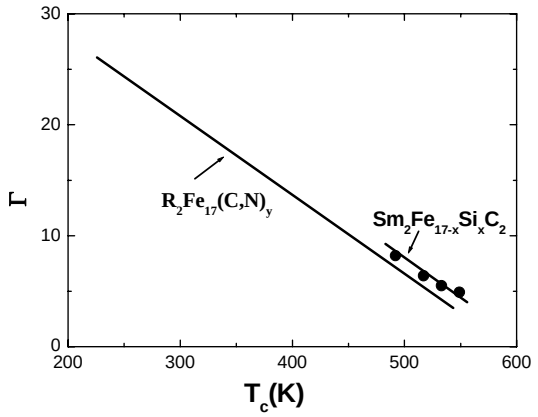

Fig. 5.The Γ values as function of T_c. By solid line are data obtained in $R_2Fe_{17}C_y$ with y ≥ 2.5.

The Γ values as function of Curie temperatures in $Sm_2Fe_{17-x}Si_xC_z$ (z = 0,2) alloys are plotted in Fig. 5. On the same figure, the Γ values obtained in $R_2Fe_{17}(C,N)_y$ compounds with y ≥ 2.5 are also given [12]. In both cases linear variations described by the relation $\Gamma = c\text{-}dT_c$ are shown. Values c = 34.5 and d = 0.054 K^{-1} were obtained for nanocrystalline $Sm_2Fe_{17-x}Si_xC_z$ system and c = 38 and b = 0.06 K^{-1} in case of $R_2Fe_{17}(C,N)_y$ one. The $\gamma = \frac{d \ln J_{eff}}{d \ln v}$ values are 16.4 in nanocrystalline Sm-Fe-Si-C and 16 in crystalline $R_2Fe_{17}(C,N)_y$ compounds. We evaluated also the γ values by using the molecular field approximation. These values were somewhat smaller (by≅20%) than those obtained from Fig.5. The differences may be attributed to the approximations used in estimating J_{eff} values by considering mean values of the iron moments as well as those involved by the molecular field model. But generally speaking, these are in rather good agreement. The linear Γ vs T_c dependence suggests that iron, in the mentioned systems, have mainly a localized behaviour. The volume variation of the exchange interactions are nearly the same, both in nanocrystalline and polycrystalline systems.

The exchange interactions between rare-earths and M (M=Fe,Co) atoms, in R_2M_{17} (M = Fe,Co) compounds, were also analysed by considering the 4f-5d-3d path. For this reason band structure calculations were performed. These allowed to determine the iron moments at various lattice sites. The dependences of iron and cobalt moments on De Gennes factor $G = (g_J\text{-}1)^2 J(J+1)$, for heavy rare compounds are plotted in Figs. 6 and 7. The data obtained in case of Sm_2Fe_{17} compound are given in Table 1. We note that heavy rare earth compounds, R_2Fe_{17}, crystallize in a hexagonal structure of $P6_3/mmc$ type, while R_2Co_{17} ones in a rhombohedral lattice of $R\bar{3}m$-type. For all lattice sites, the Fe moments are linearly dependent on De Gennes factor $M_M = M_M(0) + \alpha G$, where $\alpha = 4 \cdot 10^{-2}$ μ_B for Fe. From these data it results that fractions of (5-7) % of the iron moments are induced when replacing Y by Gd. The data are in agreement with the supposition that iron has mainly a localized moment. According to Stearns model [13], 95% of Fe3d electrons are situated in narrow d band and can be considered as localized in agreement with the analysis of volume effects. The cobalt moments are nearly constants in heavy rare-earth compounds. This implies that these are well localized. The high Curie temperatures of these systems, $T_c \cong 1200$ K, are in agreement with this assumption.

Table 1. Magnetic moments.

Compound	Magnetic moments (μ_B)				
	Sm(6c)	Fe(6c)	Fe(9d)	Fe(18f)	Fe(18h)
Sm_2Fe_{17}	-0.66	2.50	1.70	2.20	2.20

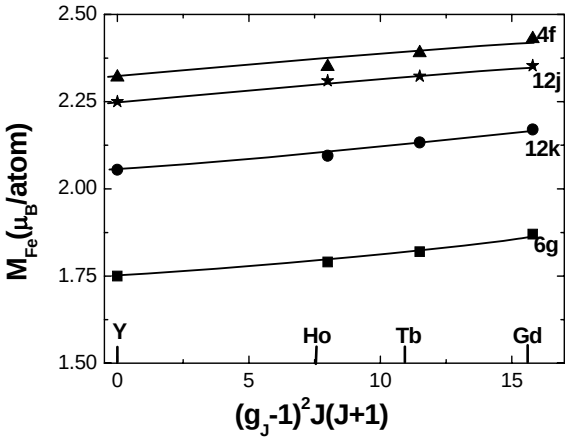

Fig. 6.Iron magnetic moments in R_2Fe_{17} heavy rare-earth compounds as function of De Gennes factor.

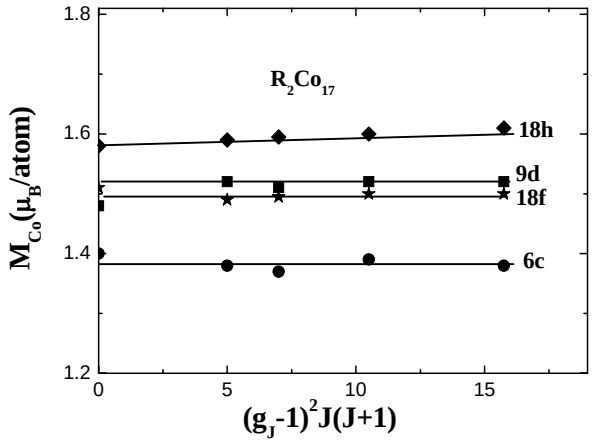

Fig. 7.Cobalt magnetic moments in R_2Co_{17} heavy rare-earth compounds as function of De Gennes factor.

The R5d band polarizations follow also linear dependences $M_{5d} = M_{5d} + \beta G$ with $\beta = 1 \cdot 10^{-2}$ μ_B for both Fe and Co compounds– Fig.8. The above data suggest the presence of two contributions. The first βG is due to local 4f-5d exchange and is nearly the same for a given R atom, independent on M metal. The $M_{5d}(0)$ values obtained by extrapolation of M_{5d} vs G dependences, at G = 0, are nearly the same as that induced on Y4d band in Y_2M_{17} compounds by 4d-3d short range exchange interactions. Consequently, this contribution was ascribed to 5d-3d short range exchange interactions. The $M_{5d}(0)$ values are dependent on the M magnetic moments. The above analysis show that the R-M exchange interactions are well described in the 4f-5d-3d model.

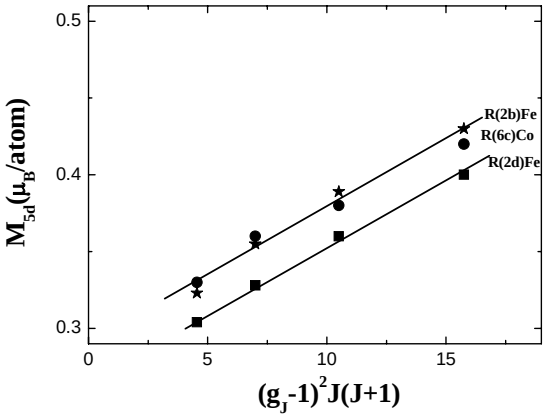

Fig. 8. R5d band polarizations in R_2Fe_{17} and R_2Co_{17} compounds as function of De Gennes

The nanocomposite alloys having low rare earth content as $Nd_6Fe_{88-y}M_yB_6$ with M = Fe, V and y=1 were studied. The reduction of the Nd concentration, as compared to 2:14:1 hard magnetic phase, provides less expensive permanent magnets. The melt spun alloys were mainly amorphous with a small amount of α-Fe and Fe_3B nanocrystallites. The hard magnetic properties were obtained by crystallization at 650^0C. The variation of remanent inductions and of coercive fields as function of thermal treatment time are shown in Figs 9 and 10. The better magnetic properties were obtained after 5 min thermal treatment. The alloys are constituted from hard magnetic 1:14:2 phase of ≅ 40 nm and soft magnetic phases having dimensions of 18 – 20 nm on the grain boundary. The remanent induction $(0.62–0.67)B_r$ are higher than predicted theoretically by Stoner-Wohlfarth model, $B_r/2$, considering randomly noninteracting particles [14]. The increase in the remanent induction, due to the nanoscale structure, is further enhanced by the presence of soft magnetic phases which have higher saturation inductions than that of the $Nd_2Fe_{14}B$ – phase.

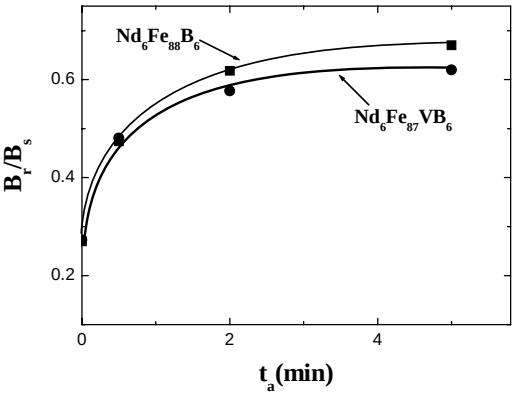

Fig. 9. Remanent inductions of $Nd_6Fe_{88-y}M_yB_6$ alloys as function of annealing time at 650 ^oC.

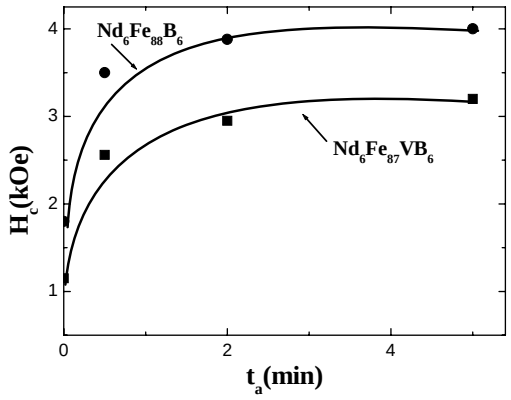

Fig. 10. Coercive fields of $Nd_6Fe_{88-y}M_yB_6$ alloys as function of annealing time at 650 ^oC

The coercive fields are rather high. Values 4 kOe and 3.2 kOe were obtained for $Nd_6Fe_{88}B_6$ and $Nd_6Fe_{87}VB_6$ alloys, respectively. The exchange coupling between soft and hard magnetic phase reduces the resistance to the reversal of magnetization and thus the coercivities. The presence of soft magnetic phase does not leads to collapse of H_c values as in a microcrystalline systems. This can be correlated with the distribution of soft magnetic phases as discrete particles smaller than the exchange distance of the phase. In the present system, the dimensions of the soft nanoparticles are higher than optimum values of ≅ 15 nm as well those of the hard magnetic phase of ≅ 30 nm. Consequently, the hard magnetic properties of the present system can be further improved by using a higher wheel speed than 25 m/s ensuring thus a full amorphisation of the as melt spun alloys.

4. Conclusion

The $Sm_2Fe_{17-x}Si_xC_2$ nanocrystalline alloys have high saturation magnetizations and Curie temperatures. The anisotropy is uniaxial. The increase of Curie temperatures as compared to noncarbonated samples was correlated with volume effects. The volume effects on the Curie temperatures and on the effective exchange interaction parameters show that iron has mainly a localized behaviour. The exchange interactions between iron atoms are of short range. The R-M (M = Fe,Co) exchange interactions are of 4f-5d-3d type. The magnetic moments of M atoms, at various lattice sites in R_2M_{17} compounds, with heavy rare earths were determined . The R5d band polarizations are due both to local 4f-5d as well as 5d-3d short range exchange interactions.

The $Nd_6Fe_{88-y}M_yB_6$ nanocomposites with M = V,Fe and y=1 show remanent inductions of (0.62-0.67)B_s. The magnetic behaviour was correlated with their microstructures formed by hard magnetic grains with d ≅ 40 nm and α-Fe and Fe_3B soft magnetic phases having d ≅ 20 nm.

Acknowledgement

The financial support from CNCSIS under grant 164/4 is gratefully acknowledged.

References

[1] C. Djega-Mariadassou, L. Bessais, A. Nandra, J. M. Greneche, E. Burzo, Phys. Rev. B **65**, 014419 (2001).
[2] C. Djega-Mariadassou, L. Bessais, A. Nandra, J. M. Greneche, E. Burzo, Phys. Rev. B **68**, 024406 (2003).
[3] L. Bassais, C. Djega-Mariadassou, A. Nandra, M. D. Appay, E. Burzo, Phys. Rev. B **69**, 064402 (2004).
[4] E. Burzo, C. Djega-Mariadassou in Nanoscale Devices-Fundamentals and Applications, Springer Verlag, 2006 p. 371-385.
[5] E. Burzo, Landoldt Börnstein Handbuch III/19i2, Springer Verlag Berlin, 1992 p. 264.
[6] E. Burzo, Rep. Progr. Phys. **61**, 1099 (1998).
[7] O. K. Anderson, Phys. Rev. **B12**, 3060 (1975); O. K. Anderson, O. Jepsen, Phys, Rev. Letters **53**, 2571 (1984).
[8] R. O. Jones, O. Gunnarson, Rev. Mod. Phys. **61**, 689 (1989).
[9] U. von Barth, L. Hedin, J. Phys. C.: Solid State Phys. **5**, 1629 (1972)
[10] S. Jaakkola, S. Parviainen, S. Penttila, J. Phys.: Metal Phys. **5**, 543 (1975).
[11] M. Brouha, K. H. J. Buschow, J. Appl. Phys. **64**, 1813 (1973).
[12] N. Plugaru, M. Valeanu, E. Burzo, IEEE Trans. Magn. **30**, 663 (1994); M. Valeanu, N. Plugaru, E. Burzo, Phys. Stat. Solidi (b) **184**, K 77 (1994).
[13] M. B. Stearns, Phys. Rev. **B8**, 4383 (1973); Physica B **91**, 37 (1977).
[14] E. C. Stoner, E. P. Wohlfarth, Phil. Trans. Royal Soc. A **240**, 579 (1948).

*Coresponding author: burzo@phys.ubbcluj.ro